KINEMATIC COMPARISON OF THE POLAR-II AND PMHS IN PEDESTRIAN IMPACT TESTS WITH A SPORT-UTILITY VEHICLE

Jason Kerrigan, Check Kam, Chris Drinkwater, Drew Murphy, Dipan Bose, Johan Ivarsson, Jeff Crandall
University of Virginia Center For Applied Biomechanics

ABSTRACT

A primary function of pedestrian dummies is the biofidelic representation of whole-body kinematics. To assess the biofidelity of a pedestrian dummy, the kinematic response of post-mortem human surrogates (PMHS) tested in full-scale pedestrian impact tests was compared with the kinematic response of the Polar-II dummy. Two PMHS were tested in full-scale pedestrian impact tests using a late-model sport-utility vehicle with an impact velocity of 40 km/h. Three additional tests using the Polar-II dummy were conducted in identical conditions to those used in the PMHS tests. Using photo targets mounted at the equivalent locations of the head center of gravity, top of the thorax, thorax center of gravity, and pelvis center of gravity, the kinematic response of the pedestrian surrogates was evaluated by comparing their parametric trajectory data. Given the significance of head impact for pedestrian injury outcome, head velocity-time signals were also compared. To provide insight into the effect of exterior vehicle geometry, the kinematic response of the Polar-II and PMHS tested using a late model small sedan were also compared with the dummy and PMHS response from the SUV tests. Comparing dummy and PMHS response, the Polar-II generally replicated the complex kinematics of the PMHS and demonstrated good overall biofidelity.

Keywords: Pedestrian Kinematics, Sport Utility Vehicles (SUV), Pedestrian Dummy

PEDESTRIANS KILLED IN pedestrian-vehicle collisions represent 65% of all road traffic fatalities worldwide (World Bank 2001). While the percentage of pedestrian fatalities is much higher in developing rather than in industrialized nations, pedestrians still make up 11%-30% of road traffic fatalities in the US, the European Union, and Japan (National Highway Traffic Safety Administration, 2003, National Police Agency, 2003, Community Road Accident Database, 2002).

To combat this public health problem, researchers have developed pedestrian dummies and pedestrian computational models to aid in further understanding pedestrian injury mechanisms and to evaluate vehicle aggressiveness to pedestrians. Numerous studies presenting data from pedestrian impact tests with different pedestrian dummies were published in the late 1970's and early 1980's (Pritz, 1978, Bourret *et al.*, 1979, Heger and Appel, 1981, Kallieris and Schmidt, 1988 and many others). More recently, most of the public research regarding the development and validation of pedestrian dummies has been with regard to one particular dummy, the Polar dummy (Akiyama *et al.*, 1999a, 1999b, and 2001, Huang *et al.*, 1999, Artis *et al.*, 2000, Okamoto *et al.*, 2001, Kerrigan *et al.*, 2005). Development of the Polar dummy began in 1997 by Honda R&D Co., Ltd. in collaboration with GESAC Inc. and the Japan Automobile Research Institute (JARI). The latest version of the Polar dummy, known as the Polar-II (Figure 1), is the result of multiple revisions targeted to improve biofidelity.

The biofidelity of the Polar-II was first evaluated at the full-scale level by comparing its response in tests with a sedan to the response of PMHS in similar tests (Akiyama *et al.*, 1999a, 1999b and 2001, Huang *et al.*, 1999). However, the PMHS tests, originally discussed by Ishikawa *et al.*(1993), were conducted using a different vehicle than that which was used in the comparison tests on the Polar-II dummy (Akiyama *et al.*, 2001). Thus, a new study (Kerrigan *et al.*, 2005) was carried out to compare the kinematic response of the Polar-II dummy and PMHS tested in full-scale pedestrian impacts using a late-model small sedan. Polar-II body segment trajectories and head velocity were compared to PMHS corridors for body segment trajectory and head velocity. Kerrigan *et al.* (2005) concluded that the Polar-II dummy generally mimicked the complex upper-body kinematics of the PMHS and demonstrated good overall biofidelity in full-scale impact tests with a small sedan (when the dummy

and PMHS are positioned lateral to the vehicle, along the vehicle's centerline, and in a mid-stance position). However, it has long been hypothesized that pedestrian kinematic response is highly sensitive to the geometry of the impacting vehicle. To evaluate this kinematic sensitivity to vehicle geometry, full scale pedestrian impact experiments with the Polar-II dummy were conducted using six different vehicles: three different sport-utility vehicles (SUVs), a mini car with a high hood leading edge, and two passenger vehicles (Akimaya *et al.*, 2001 and Okamoto *et al.*, 2001). The studies showed that dummy head trajectory, velocity, and wrap-around-distance (WAD) to head strike in SUV impacts are different than in passenger car impacts.

Fig. 1. Polar-II dummy (left) with posterior (center) and lateral (center-right) views of the left knee joint and the flexible tibia (right)(Akiyama *et al.*, 2001, Takahashi *et al.*, 2005).

Understanding how pedestrian kinematics are influenced by vehicle geometry is crucial in reducing pedestrian injury and fatality since the vehicle fleet constantly changes. By 1999, light trucks, vans, and sport-utility vehicles (LTVs) had accounted for 50% of all US vehicle sales (Longhitano *et al.*, 2005). Even though there are substantially fewer LTVs in the European fleet, the acceptance tests for pedestrian protection proposed by the European Enhanced Vehicle-Safety Committee (EEVC) include a modification for high-bumper vehicles (EEVC, 1998).

Additionally, the mechanisms of pedestrian injury have also been shown to be sensitive to vehicle geometry. A recent epidemiological study suggests that although the most frequently injured body region in all pedestrian victims was the head, but that the second most frequently injured body region in pedestrians struck by passenger vehicles is the lower extremity, whereas it is the torso for those struck by SUVs (Longhitano *et al.*, 2005). Pedestrians struck by LTVs (as opposed to passenger cars) have also been shown to be twice as likely to sustain brain, thoracic, and abdominal injuries when the impact speed is less than 48 km/h (Ballesteros *et al.*, 2004).

While kinematic and injury sensitivity to vehicle geometry have been previously shown, there have been no public research studies presenting full-scale pedestrian impact studies on PMHS with LTVs. Thus full scale pedestrian impact tests with both PMHS and the Polar-II dummy were performed using a late-model SUV to both evaluate the kinematic biofidelity of the Polar-II dummy in impacts with an SUV, and to compare PMHS and Polar-II kinematics between a late-model SUV and a late-model small sedan.

FULL-SCALE TEST METHODOLOGY

Two full-scale pedestrian impact experiments were conducted by impacting PMHS with a late-model SUV (developed for the US market), and three tests were conducted by impacting the Polar-II dummy with the same SUV. All vehicle damage was repaired after each test and all test conditions remained identical in all five tests to minimize variability in the results and facilitate biofidelity evaluation of the Polar-II dummy.

SLED SYSTEM : The SUV (Figure 2) was cut in half at the B-pillar and mounted on a sled fixed to the deceleration sled system at the University of Virginia (UVA) Center for Applied Biomechanics. A hydraulic decelerator was positioned at the impact end of the sled to stop the vehicle at the end of the vehicle-surrogate (dummy or PMHS) interaction.

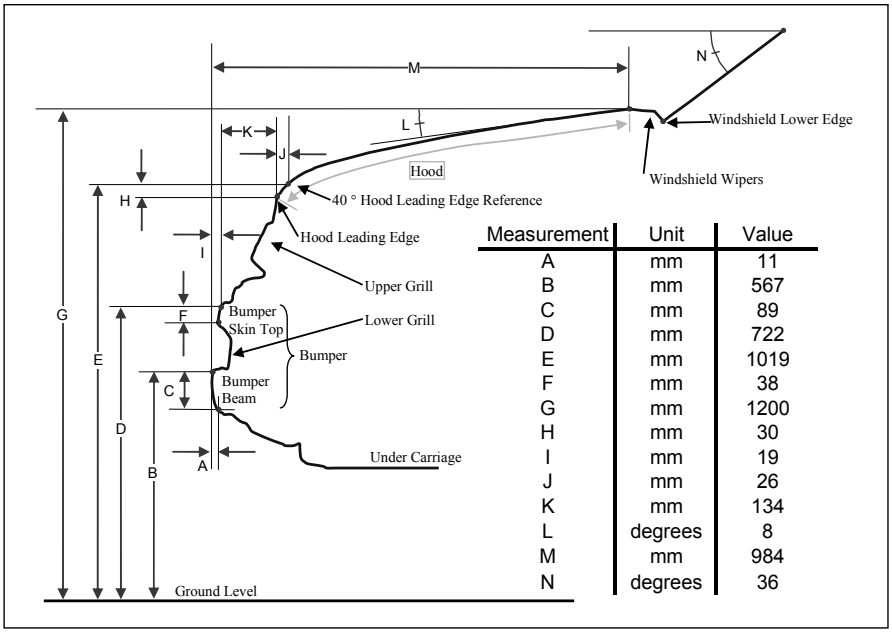

Measurement	Unit	Value
A	mm	11
B	mm	567
C	mm	89
D	mm	722
E	mm	1019
F	mm	38
G	mm	1200
H	mm	30
I	mm	19
J	mm	26
K	mm	134
L	degrees	8
M	mm	984
N	degrees	36

Fig. 2. Scaled dimensioned drawing of the center-line contour of the SUV used in this study.

A small, light pedestrian sled was constructed to act as the ground-reference-level for the pedestrian surrogate and to facilitate surrogate positioning prior to each test. Plywood, which has been shown to possess frictional characteristics similar to road surface (Kam *et al.*, 2005), was used as the shoe-contact surface on the ground-reference-level. The pedestrian sled was positioned in a location relative to the hydraulic decelerator that permitted the vehicle to interact with the pedestrian surrogate for approximately 250 ms between the time of primary vehicle-surrogate contact ("bumper contact"), and the initiation of vehicle deceleration (Figure 3, and Kam *et al.* 2005).

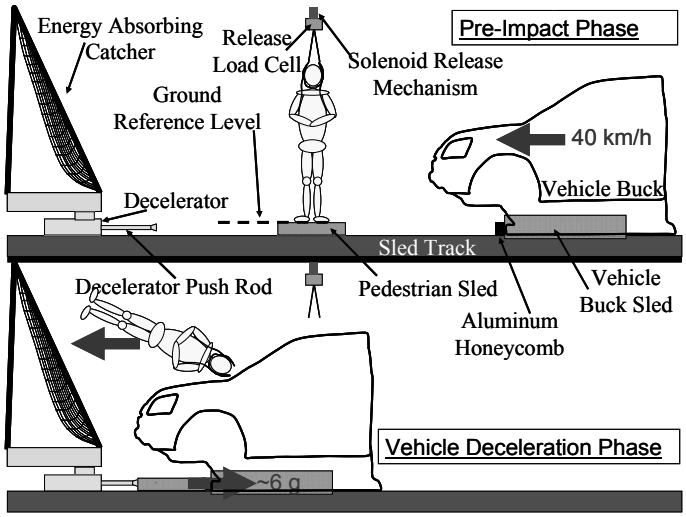

Fig. 3. Schematic of full-scale pedestrian impact test setup. In the pre-impact phase, the vehicle is accelerated to 40 km/h. In the vehicle deceleration phase (after the pedestrian surrogate interaction phase) the vehicle deceleration causes the surrogate to be thrown into the energy absorbing catching structure. Schematic is not to scale.

In vehicle-to-pedestrian collisions, pedestrians often incur additional injuries during impact with the ground, road structures or other vehicles after being struck by the primary vehicle. In this study, however, the focus remains solely on interaction with the primary vehicle. Since vehicle deceleration causes the surrogate to be thrown off the front of the vehicle, a catching mechanism was installed at the end of the sled tracks (Figure 3, and Kam *et al.*, 2005).

PMHS AND DUMMY PREPARATION : One male and one female PMHS (Table 1) were selected for this study based on the absence of pre-existing fractures, lesions or other bone pathology

(as confirmed by CT scan). The PMHS were preserved by a combination of refrigeration and freezing (Crandall, 1994). Both PMHS were obtained and treated in accordance with the ethical guidelines approved by the Human Usage Review Panel, National Highway Traffic Safety Administration, and all PMHS testing and handling procedures were approved by the UVA institutional review board.

Table 1. Description of the PMHS used in this study.

Test #/ PMHS ID	Age at Death/ Gender	Post Mortem Stature[1] (mm)	Stretched Stature[2] (mm)	Height Change[3] (%)	Weight (kg)	Cause of Death
C4/213	75/F	1676	1765	5.3%	46.7	Polycythemia Vera
C5/233	53/M	1715	1760	2.7%	104.2	Cardiac Arrest

1- Height measured post-mortem with each PMHS lying supine.
2- Height measured by scaling a video image of PMHS in pre-test gait-like striding position.
3. Height change is a measure of change in PMHS stature caused by vertically supporting the PMHS by the upper body.

Preparation of PMHS specimens involved fixing instrumentation plates to the head, first thoracic vertebra (T1), eighth thoracic vertebra (T8) near the thorax center of gravity (CG), and sacrum near the pelvis CG. Instrument cubes were mounted to the instrument plates and served as anchors to install photo targets used for video analysis. Mounts were used at equivalent locations on the dummy as anchors for photo targets. More detail regarding the procedures performed during PMHS and dummy preparation can be found in Kerrigan *et al.* (2005).

SUPPORT : After the dummy and PMHS were prepared, they were outfitted with harness straps for subsequent positioning. In the dummy, the harness consisted of a rope that was tied through the eye bolts on the shoulders of the dummy (Figure 1 and 4, and Kerrigan *et al.*, 2005). The harness for the PMHS consisted of two sections of seatbelt webbing. One longer piece (the shoulder strap) was directed under the arms of the PMHS anteriorly and across the posterior thorax. The second seatbelt strap was split longitudinally in the middle so that half of the strap could be positioned under the PMHS chin and the other half could slip under the occiput (Figure 4 and Kerrigan *et al.*, 2005). The lengths of the two harness straps used in the PMHS tests were such that the majority of the weight of the PMHS was supported by the shoulder strap. The head strap was only used to keep the head in a neutral position.

When the surrogate was hoisted into position over the pedestrian sled, support of the surrogate's weight was transferred to the clamp of a solenoid release mechanism. The release mechanism supported the weight of the surrogate until immediately prior to the impact when clamp opened and the surrogate was released. A load cell mounted above the release mechanism was used to determine the exact time of release.

POSITIONING : Data from the pedestrian crash data study (PCDS) suggest that the majority of pedestrians are struck laterally with their lower extremities positioned in a gait-like orientation (Kam *et al.*, 2005). Thus, all surrogates in this study were positioned laterally along the vehicle-center-line in a mid-stance position (Figure 4). The arms of the surrogate were bound at the wrist to ensure repeatable kinematics and the most severe impact (Kam *et al.*, 2005).

TEST EVENT : Once the final position of the surrogate had been set and measured, the test event was initiated by accelerating the vehicle sled up to 40 km/h. The vehicle sled passed an inductive sensor on the track that triggered the release of the surrogate between 19 and 28 ms before the initial bumper contact. After both of the surrogate's feet were no longer in contact with the ground-reference-level on the pedestrian sled (about 50 ms after bumper contact), the vehicle impacted and accelerated the pedestrian sled. Approximately 200 ms later, both sleds, now coupled together, contacted the decelerator (Figure 3). At 250 ms after initial bumper contact, the vehicle deceleration phase began and the surrogate was thrown forward into the catching mechanism.

KINEMATICS MEASUREMENT

Pedestrian surrogate upper body kinematics measurement was performed by tracking the motion of photo targets on the pedestrian surrogates using images from a high speed video imager (Phantom V5.0, Vision Research, Wayne, NJ). The imager sampled a 1024 by 1024 pixel array at 1000 Hz and was positioned off-board on the vehicle left-hand side during all of the tests. Representative test images are given in Figure 5.

Fig. 4. Typical dummy (Left) and PMHS (Right) orientations prior to each test. The bag attached to the dummy's lumbar area and the PMHS left-side pelvis area contains a data acquisition system used to sample data from sensors mounted on the dummy and PMHS (see Kerrigan *et al.*, 2005).

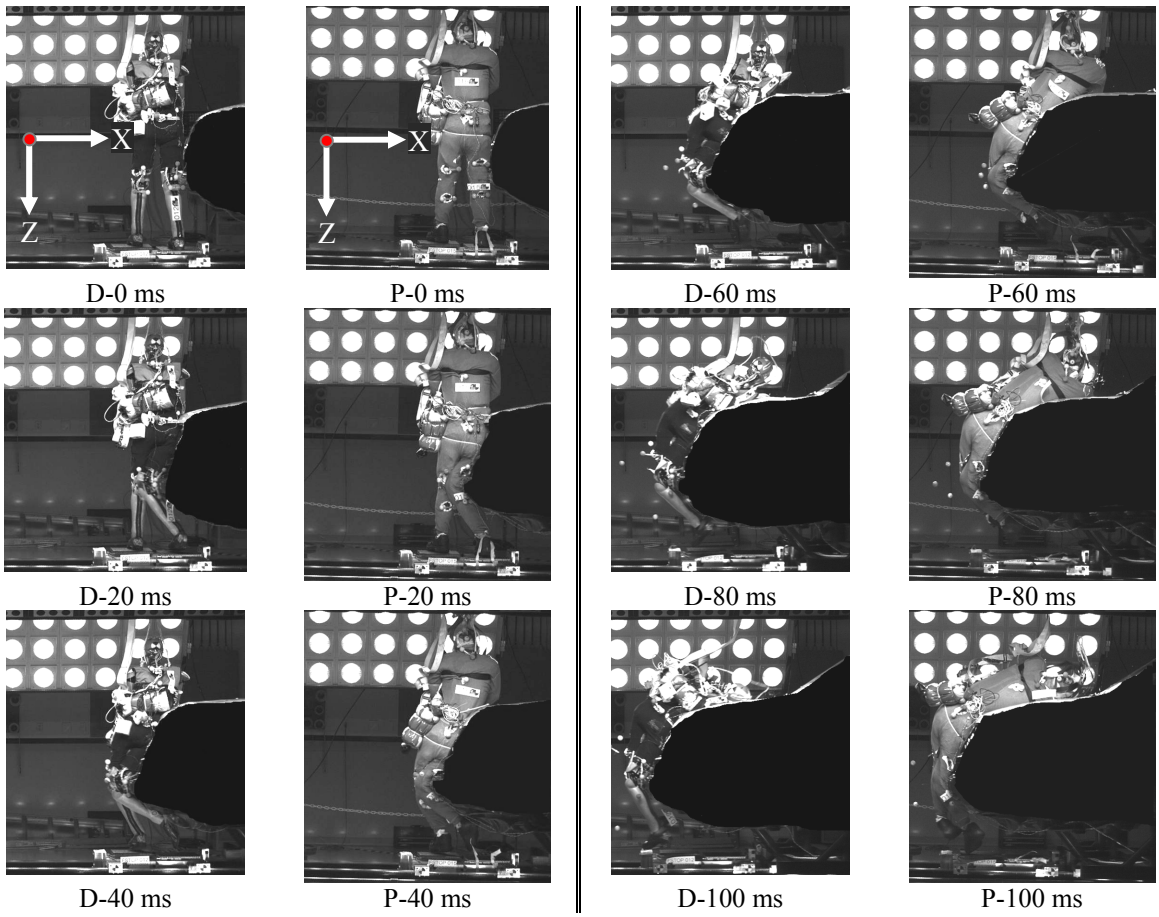

Fig. 5. High speed digital video images from a typical dummy (left, denoted by "D-") test and PMHS (right, denoted by "P-").

All of the photo targets, target locations, mounting methods, and sampling/processing methodology are the same as discussed in detail by Kerrigan *et al.* (2005). While detail regarding data processing methodology is presented here, only an overview of the video analysis procedures is given.

Photo targets were securely mounted at equivalent locations on the PMHS and dummy at the posterior projection of the head CG, at the top of the thorax (T1), thorax CG (T8), and pelvis CG. For each analysis frame, selected as every fourth video frame, the position data for each target were recorded. The time of initial bumper contact was defined to be the beginning of the event, t=0, and the time of head strike, t_{hs}, marked the end of the event (Kam *et al.*, 2005). The t_{hs} was determined by inspection of the video and rounded to the nearest 4 ms interval so that it corresponded to an analysis frame. The analysis frame at $t=t_{hs}$ + 20 ms was the last frame digitized (Table 2).

DATA ANALYSIS : The trajectory data were recorded in the frame coordinate system (FCS), which was defined by the view of the high speed imager and fixed with respect to the laboratory. The x' and z' directions (FCS quantities are denoted by the prime " ′ ") were defined as the horizontal and vertical axes of the imager frame, respectively. The $+x'$ axis pointed to the right and $+z'$ axis points downward (Figure 5).

Table 2. Time of head strike, digitized frame closest to the time of head strike, and last frame digitized for each test.

	Dummy			PMHS	
Test	**D-4**	**D-5**	**D-6**	**C-4**	**C-5**
Time of Head Strike (ms)	101	96	95	97	99
Head Strike Imager Frame	100	96	96	96	100
Last Frame Analyzed	120	116	116	116	120

The parametric trajectories ($x'(t)$ and $z'(t)$ for each target) were first converted from pixels to mm by multiplying each surrogate signal by 3.695 mm/pixel and the vehicle signal by 3.243 mm/pixel. These values for the spatial resolution of the imager at the surrogate plane and at the left-hand side vehicle exterior plane were determined prior to the test. The filtering convention specified in ISO/DIS 13432-4 (ISO, 2004) was adopted to smooth the position data:

$$x'_i = \frac{1}{4}\left(x'_{i-1} + 2x'_i + x'_{i+1}\right) \qquad z'_i = \frac{1}{4}\left(z'_{i-1} + 2z'_i + z'_{i+1}\right) \qquad (1).$$

Four passes of the filter in Equation 1 were applied to each target's trajectory (ISO, 2004).

The trajectories were then converted to the vehicle coordinate system (VCS), which was defined to be fixed with respect to the vehicle. In the vehicle coordinate system, the $+z$ axis pointed down and the +x axis pointed horizontally from the front to the back of the car (VCS quantities are given without the prime " ′ " to distinguish them from FCS quantities). The origin of the VCS is defined by the location of the surrogate's head CG photo target at the t=0 frame in the x direction, and by the ground-reference-level in the z direction.

The coordinate transformation from the FCS to the VCS is given by Equation 2:

$$x_i = s_x + \left(x'_i - x_v{}'_i\right) - \left(x'_0 - x_v{}'_0\right) \qquad z_i = s_z + \left(z'_i - z_v{}'_i\right) - \left(z'_0 - z_v{}'_0\right) \qquad (2).$$

In Equation 2, all terms are in mm and,

- x_i, and z_i are the x and z positions (VCS) of each surrogate target, at frame i,
- $x_v{}'_i$ and $z_v{}'_i$ are the x and z positions (FCS) of the vehicle photo target at frame i,
- $x_v{}'_0$ and $z_v{}'_0$ are the same as $x_v{}'_i$ and $z_v{}'_i$, except at the t=0 frame,
- x'_0 and z'_0 are the x and z positions (FCS) of each surrogate target at the t=0 frame, and
- s_x, and s_z are the x and z coordinates (VCS) of each body segment's photo target at the t=0 frame.

Next, the component velocities of the head were calculated to compare PMHS and dummy kinematic response in the temporal regime, as well as the head velocity at head strike. The velocity of the head was calculated by adopting the centered difference derivative method used in ISO/DIS 13232-5 (ISO, 2004) and given by Equation 3:

$$V_{x,i} = \frac{x_{i+1} - x_{i-1}}{t_{i+1} - t_{i-1}} \qquad V_{z,i} = \frac{z_{i+1} - z_{i-1}}{t_{i+1} - t_{i-1}} \qquad (3).$$

In Equation 3,

- $V_{x,i}$, $V_{z,i}$ are the x and z components (VCS) of the head velocity, at frame i, in m/s, and
- t_i is the time, in ms, at frame i.

The resultant of the velocity signal is then computed by calculating the magnitude of the velocity vector defined by the velocity components (Equation 3).

Both Equation 3 and Equation 1 require data from future times to calculate signals at the current time step. Since the head velocity abruptly decreases after head strike due to contact with the vehicle, Equation 3 could underestimate the velocity at head strike. Therefore the motion of the head over each of five 4 ms intervals (20 ms total) after the head strike frame is assumed to be the same as in the 4 ms interval prior to the head strike frame.

SURROGATE KINEMATICS : The trajectories of the head CG, T1, T8, and pelvis in the VCS (Equation 2) are given for the PMHS tests in Figure 6. To provide an indication of relative body segment motion, lines connecting each pair of adjacent body segments are depicted at 12 ms time intervals ("Body Segment Linkage" in Figure 6). Each trajectory is plotted from time t=0 to the time of head strike (see Table 2 above). The head velocities calculated in Equation 3 are plotted for both PMHS tests in Figure 7. The dummy upper body trajectory data and head velocity data (Figure 8) show good repeatability.

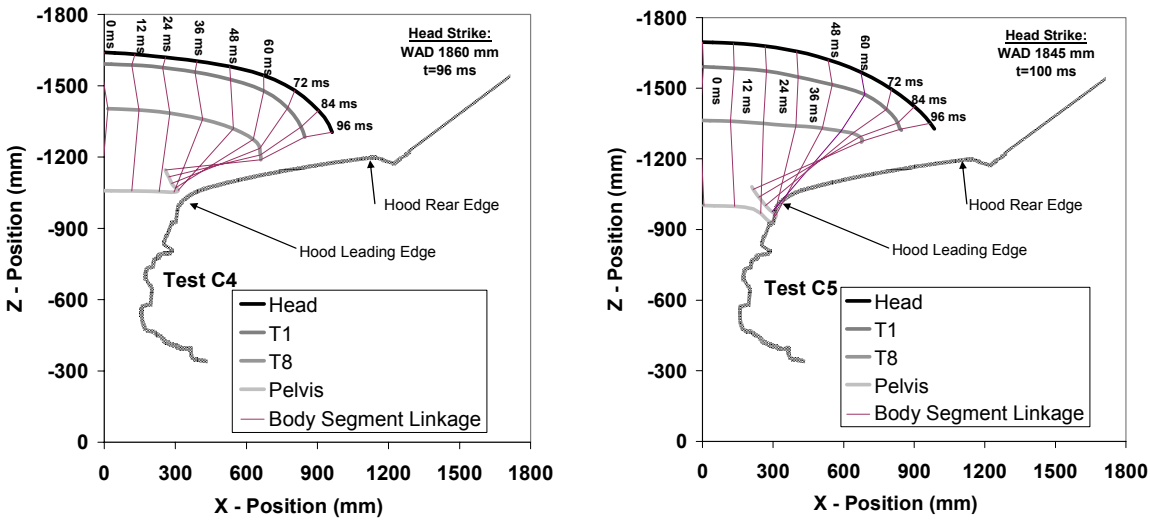

Fig. 6. PMHS body segment trajectories for tests C4 (left) and C5(right). The vehicle center-line contour is added to provide a reference. The origin of the VCS is depicted in the bottom left corner of each graph.

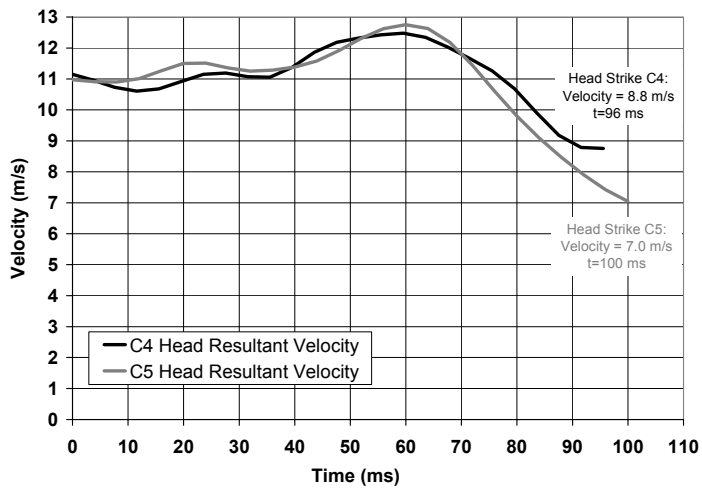

Fig. 7. Head resultant velocity time histories in the XZ plane for the PMHS in this study.

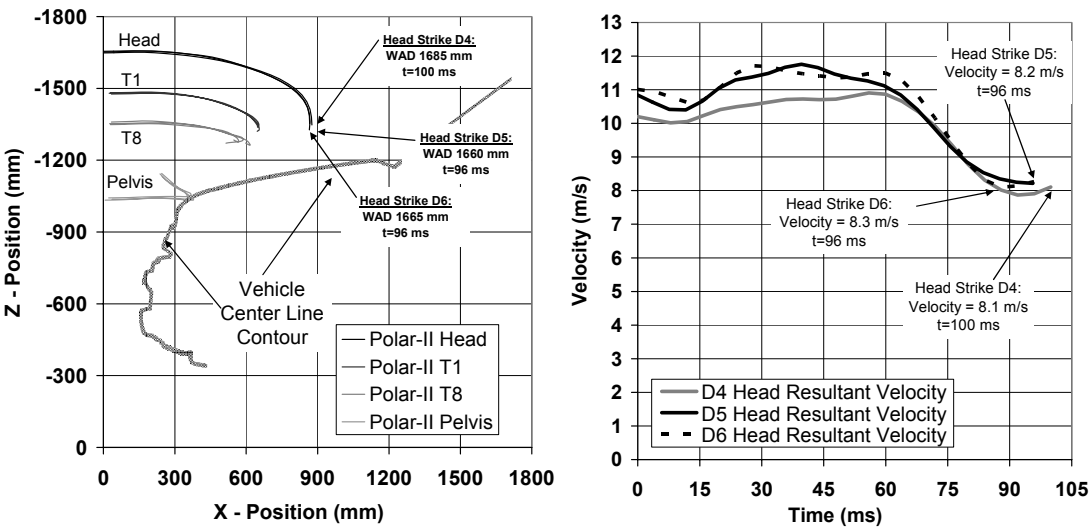

Fig. 8. Polar-II kinematic trajectories (left) and head resultant velocity time histories (right) for all three tests.

COMPARING DUMMY AND PMHS KINEMATICS FOR THE SUV

SCALING PMHS KINEMATICS DATA : The PMHS kinematics data were then scaled to a reference geometry to facilitate comparison of surrogate kinematics. The Polar-II was chosen as the reference geometry to eliminate the need to scale the dummy kinematics for comparison with the PMHS.

Recognizing that PMHS body-segment lengths vary slightly from PMHS to PMHS, and that the lengths of the Polar-II body segments are slightly different than those of the PMHS (Table 3), individual scale factors were used to scale trajectory data from each body region. Specifically, eight individual scale factors were calculated to scale each of the four body segment trajectories (head CG, T1, T8 and pelvis) for each of the two PMHS (Table 3). The scale factors were determined by dividing the average initial height of each dummy photo target by the height of the corresponding PMHS photo target (Kerrigan *et al.*, 2005). The filtered surrogate trajectory data, x'_i and z'_i, (from Equation 1) were then multiplied by their respective scale factors to obtain the scaled FCS trajectories x'^*_i and z'^*_i (scaled values are denoted by an asterisk " * "). Although the PMHS trajectories were geometrically scaled, it was impossible to scale the vehicle geometry, and thus the vehicle's motion was not scaled. Thus, the coordinate system transformation (to the VCS) becomes:

$$x_i^* = s_x\lambda + \left(x'^*_i - x_v{}'_i\right) - \left(x'^*_0 - x_v{}'_0\right) \qquad z_i^* = s_z\lambda + \left(z'^*_i - z_v{}'_i\right) - \left(z'^*_0 - z_v{}'_0\right) \qquad (4).$$

In Equation 4, λ is the length scale factor for the trajectory undergoing the coordinate transformation.

Table 3. Initial vertical distance of each body segment's photo target, PMHS length scale factors, and scaled head strike times. The far right column represents the lowest of the scaled times for each body region.

	Photo Target Initial Heights				Scale Factors		Scaled Head Strike Times t^*_{hs}		
	Dummy Mean (D4-D6) (mm)	Dummy Range (D4-D6) (mm)	Test C4 (mm)	Test C5 (mm)	Test C4	Test C5	Test C4 (ms)	Test C5 (ms)	$t^*_{hs,c}$ (ms)
Head CG	1655	7	1641	1696	1.0090	0.9760	96	96	96
Top of Thorax (T1)	1480	4	1593	1591	0.9296	0.9307	88	92	88
Thorax CG (T8)	1356	7	1404	1363	0.9658	0.9946	92	100	92
Pelvis CG	1039	13	1059	1001	0.9814	1.0375	92	104	92

Since the position of each body segment in each analysis frame was scaled, the time at each analysis frame also had to be scaled. Since a different scale factor was used at each analysis frame to scale each of the four trajectories (in each test), four different values for the scaled time at frame i, t^*_i, were calculated at each analysis frame. Since time scales the same as length, t_i was multiplied by each

of the scale factors to obtain each of the t^*_i values at each frame. Furthermore, the time of head strike, t_{hs}, was scaled to $t^*_{h,s}$, which created a different time marking the end of the event for each trajectory (Table 3).

The scaled head velocity in the VCS is defined as the difference between the scaled head velocity and the un-scaled vehicle velocity (both measured in the FCS). The scaled head velocity components (FCS), $V_h'_x$ and $V_h'_z$, were calculated by estimating the derivatives (using Equation 3) of the scaled FCS trajectories, x'^*_i and z'^*_i, with respect to scaled time, t^*_i. Since the same scale factor appeared in both the numerator and the denominator of the derivative formula, the FCS head velocity at each analysis frame was not affected by scaling. However, since the time at each analysis frame was affected by scaling, the scaled FCS head velocity components, $V_h'_x(t^*_i)$ and $V_h'_z(t^*_i)$, were functions of scaled time. The FCS vehicle component velocities, $V_v'_x(t_i)$ and $V_v'_z(t_i)$, were also calculated by differentiating the FCS vehicle trajectories, $x_v'_i$ and $z_v'_i$, with respect to time, t_i (with Equation 3). Then with both the scaled FCS head velocities and the FCS vehicle velocities, the scaled VCS head velocities, $V^*_{hx}(t_i)$ and $V^*_{hz}(t_i)$, were calculated by subtraction (Equation 5).

$$V^*_{hx}(t_i) = V_h'_x(t^*_i) - V_v'_x(t_i) \qquad V^*_{hz}(t_i) = V_h'_z(t^*_i) - V_v'_z(t_i) \tag{5}$$

Before this subtraction could occur, the scaled component head velocities ($V_h'_x(t^*_i)$ and $V_h'_z(t^*_i)$) had to be re-sampled in time by interpolation because scaling the time at each analysis frame changed the sampling interval from 4 ms to 4λ ms. The resultant of the scaled head velocity in the VCS was obtained by computing the magnitude of the scaled velocity vector defined by the parametric components in Equation 5.

CORRIDOR DEVELOPMENT : In the previous study, it was determined that trajectory data from a small sample size (n=3) did not have enough variation to justify the development of corridors based on the standard deviation of the trajectories for a dummy biofidelity evaluation (Kerrigan *et al.*, 2005). Thus, with only two PMHS tests in the current study, corridors founded on data variation were avoided and box-type corridors based on average trajectory path length were developed for the body segment trajectories. Corridors based on head velocity data were not developed.

Average Curves : Before developing corridors, it was necessary to determine an average trajectory for each body segment. The scaled trajectory data had to be re-sampled in time by interpolation so that the positions of each body segment were given on the same time scale across the two tests. The average scaled PMHS trajectories were computed by averaging the position of each body segment over the two tests at each time step (Figure 9). The average trajectories are plotted from the time of initial bumper contact (t=0 ms) to the lowest time of head strike for each body region, $t^*_{hs,c}$ (Table 3).

Upper and Lower Bounds : The path length of each body segment trajectory at frame i, S_i, was defined as:

$$S_i = \sum_{j=0}^{i} \sqrt{\left(\bar{x}^*_j - \bar{x}^*_{j-1}\right)^2 + \left(\bar{z}^*_j - \bar{z}^*_{j-1}\right)^2} \tag{6}$$

In Equation 6, $\bar{x}^*_i$, and $\bar{z}^*_i$, are the averaged scaled x and z components of each body segment's trajectory, in mm. Boxed-corridors were developed by constructing a box around each data point on the averaged curve, with edges parallel to the VCS axes. The length of each side of the box was equal to $2kS_i$, where k is some percentage of the trajectory's path length. Two pairs of parametric equations were used to define the location of the corners of the box circumscribing each point on the average trajectory:

$$\begin{aligned} x^+_i &= \bar{x}^*_i + kS_i \qquad & z^+_i &= \bar{z}^*_i + kS_i \\ x^-_i &= \bar{x}^*_i - kS_i \qquad & z^-_i &= \bar{z}^*_i - kS_i \end{aligned} \tag{7}$$

In Equation 7, x^+_i, gives the curve formed by adding the x component of the average parametric body segment trajectory at frame i to k percent of the path length at frame i. x^-_i, z^+_i, and z^-_i provide similar curves. By plotting each x curve with respect to each z curve (Equation 7), the trajectories of the four corners of each corridor box can be plotted in the VCS. The upper and lower bounds of the

corridor were given by the trajectories of two opposing corners of the corridor box. The pair of corners used as the upper and lower corridor bounds are chosen such that the angle between the tangent vector to the trajectory and the normal vector to the line connecting the corners is less than 90° (Lessley *et al.*, 2004, Kerrigan *et al.*, 2005) (Figure 10).

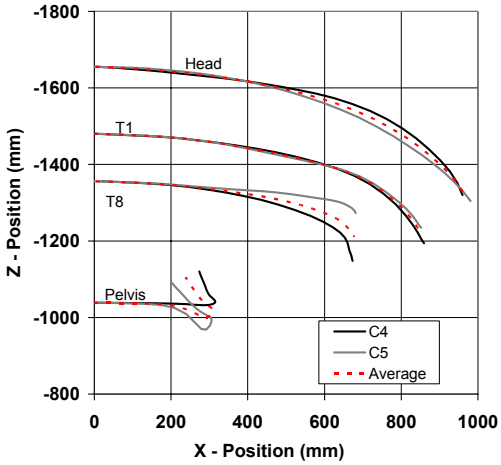

Fig. 9. Scaled trajectories from PMHS tests C4 and C5 with the average trajectories for each body region. Note that this is a magnified view and the scale of the Z-position axis does not go all the way to zero.

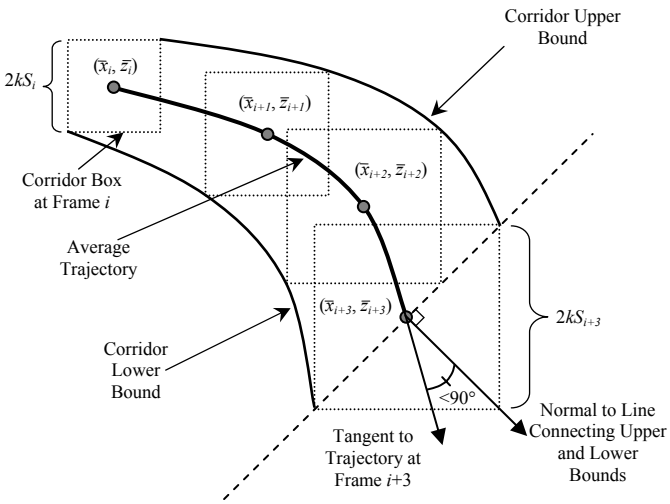

Fig. 10. Corridor development schematic. The trajectories of two opposing corners of each corridor box were used to define the upper and lower bounds of the corridor. The curvature of the average trajectory determines which pair of opposing corners is used. The corners were chosen such that the normal to the line connecting them was less than 90 degrees from the tangent to the trajectory.

The concavity of the head, T1 and T8 average trajectories remains constant from initial bumper contact to head strike so the upper right corner (z^-_i vs. x^+_i) and the lower left corner (z^+_i vs. x^-_i) of the box form the upper and lower trajectory bounds (Figure 11). The concavity of the pelvis average trajectory does not remain constant (actually concavity does not even apply since dz/dx and d^2z/dx^2 are not continuous). Thus the corners of the box that are used as the upper and lower corridor bounds have to change each time the trajectory changes concavity. To prevent narrowing of the corridor or sharp corners in the boundaries, the upper and lower bounds were smoothed over the region during transition between corners of the box when the concavity changes (Figures 12 and 13). Although no PMHS head velocity corridor is developed for comparison with the dummy velocity, the head resultant velocities for all five tests were plotted together for comparison (Figure 14).

COMPARING KINEMATICS BETWEEN THE SMALL SEDAN AND THE SUV

Differences in vehicle geometry between a sedan and an SUV have already been shown to affect Polar-II upper body kinematics (Akiyama *et al.*, 2001, Okamoto *et al.*, 2001). A similar sensitivity to vehicle geometry seemed likely for PMHS. Additionally, a further validation of the Polar-II could be performed by comparing the dummy's sensitivity to vehicle geometry with PMHS' sensitivity to vehicle geometry. Therefore, kinematics data from the current study (using the SUV) were compared with PMHS and Polar-II kinematics data from the previous small-sedan study (Kerrigan *et al.*, 2005) (Figure 15).

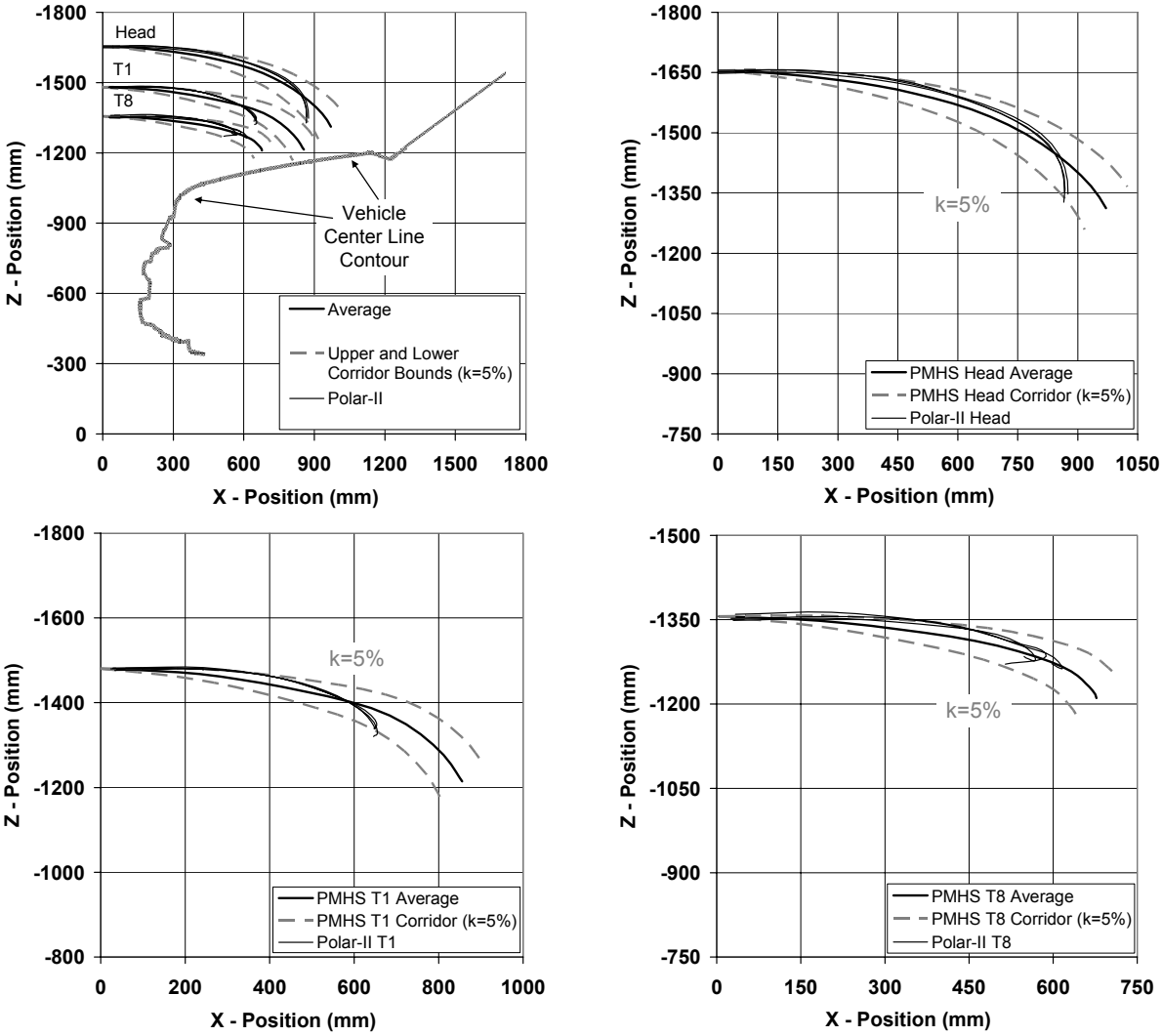

Fig. 11. An overview of the PMHS trajectory corridors (k=5%) (with average trajectories) and dummy trajectories is given (top left) with detailed views of the head (top right), T1 (bottom left) and T8 (bottom right) trajectory data. Note that the scales in each of the four plots are different.

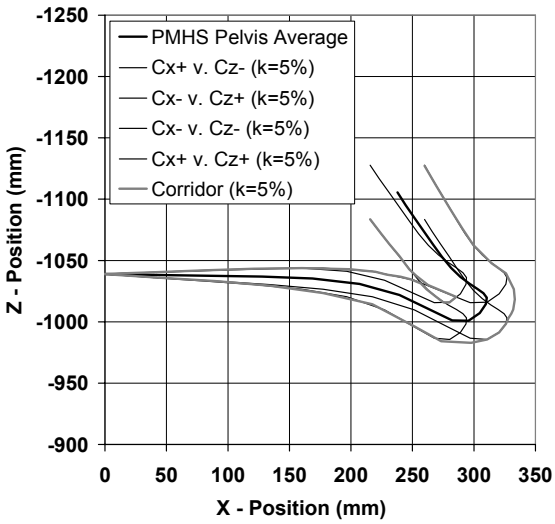

Fig. 12. Corridor bounds for the PMHS pelvis trajectory. The pair of corridor-box corners that defined the upper and lower corridor bounds changed when the average curve changed (this occurs twice). The corridor boundaries were smoothed in the transition areas.

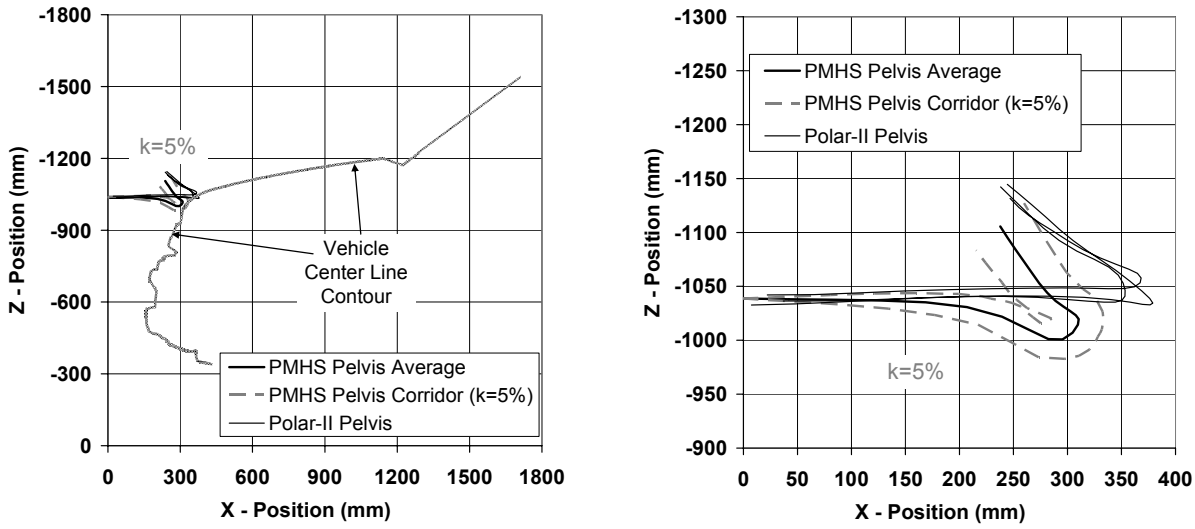

Fig. 13. Scaled PMHS pelvis average trajectory, *k*=5% corridor, and dummy trajectories are shown as an overview (left) and in detail (right).

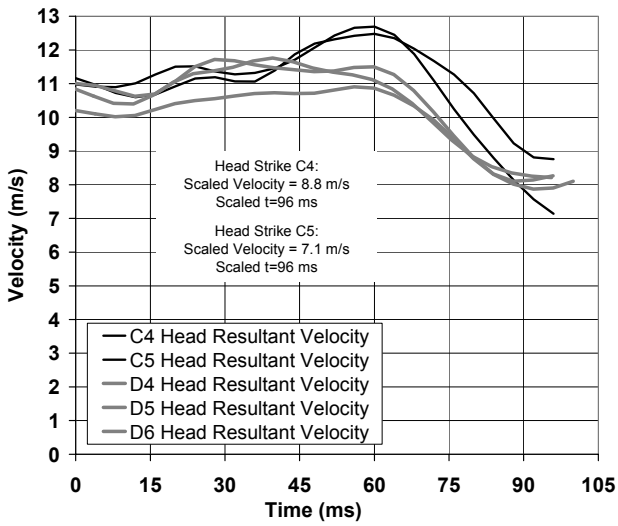

Fig. 14. Dummy and scaled PMHS head velocity time histories.

DISCUSSION

In the current study, full-scale pedestrian impact tests were performed on PMHS (n=2) and the Polar-II pedestrian dummy (n=3) using a late-model SUV traveling at 40 km/h. Photo targets were mounted at equivalent locations in the PMHS and the dummy: posterior projection of the head CG, top of the thorax at T1, posterior projection of the thorax CG at T8, and posterior projection of the pelvis CG on the sacrum. The motion of the surrogate body segments were tracked throughout the vehicle-pedestrian interaction and converted into kinematic trajectories in a reference frame fixed with respect to the vehicle. The PMHS trajectories were then scaled and averaged and corridors were developed to provide a basis for kinematic comparison of all tests.

To make an assessment of the kinematic repeatability of the dummy, the individual dummy test responses were analyzed (Figure 8). The upper-body trajectory data and head velocity data are in good agreement between tests. Additionally, the head resultant velocity at head strike had low variability between tests (8.1-8.3 m/s). The head velocity time history for test D4 appears lower than the other curves for the first 65 ms, but aligns with the other curves for the final 35 ms. A problem with the sled system rendered the speed of the vehicle during test D4 to be only 37.6 km/h. However, the difference in vehicle velocity did not affect the upper body trajectories or the resultant head velocity at head strike.

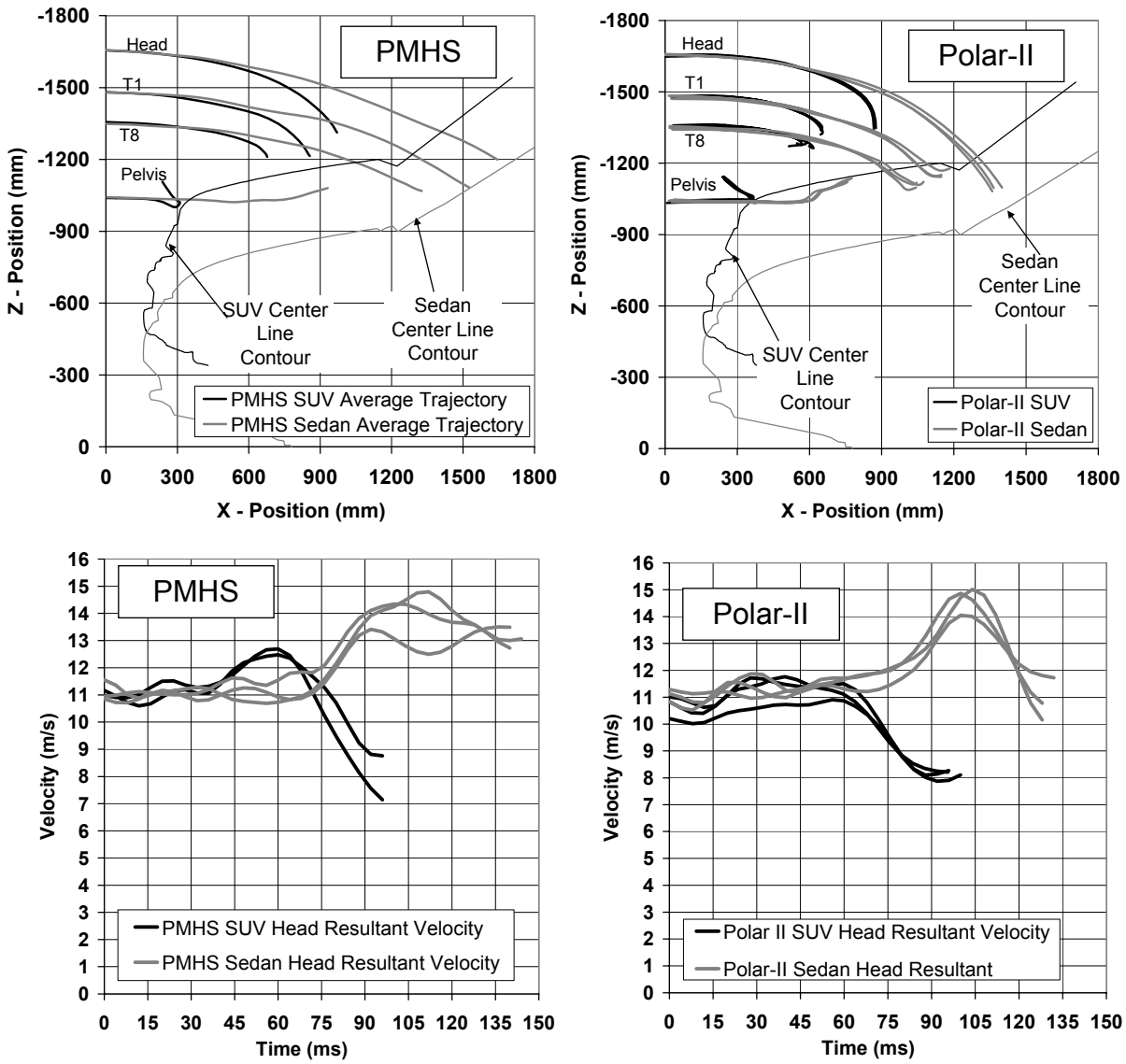

Fig. 15. Kinematics comparison for both the PMHS and Polar-II between tests with a small sedan and tests with an SUV. All PMHS data have been scaled using the procedures discussed above.

Comparison of the kinematic response by each of the two PMHS specimens highlights the sensitivity of upper body kinematics to variation in anthropometry (Figures 6 and 7). The PMHS used in test C4 had a greater stature than the PMHS used in C5 but when they were positioned before the test, they were supported by their upper bodies causing spinal stretching. This resulted in both specimens having similar stretched stature (1760-1765 mm). This similarity in initial stature likely explains the similarity in the shapes of the PMHS head and T1 trajectories, as well as the WADs to head strike (1845-1860 mm) (Figure 9). However, there is a discrepancy in the shape of the two T8 and pelvis trajectories between the two PMHS (Figure 9). In test C4, the pelvis strikes the hood leading edge and slides up onto the front end of the hood. In test C5, the pelvis first digs into the upper grill area of the vehicle before sliding up over the hood leading edge. This phenomenon is likely caused by a combination of differences in pelvis initial height and body mass. Since the initial height of the pelvis CG in C5 (1001 mm) is less than that of the hood leading edge (1019 mm), the pelvis penetrates into the upper grill below the hood leading edge before sliding up onto the hood (Figure 6). But the initial height of the pelvis CG in PMHS C4 (40 mm higher than the hood leading edge) and its relatively low mass (46.7 kg) likely permitted the pelvis to hit the hood leading edge, and slide up onto the hood much faster than in the C4 test. As a result, the pelvis in C4 ends up being much higher at the time of head strike than the pelvis in C5. Additionally, it appears that more *x-z* rotation (head is lower

with respect to pelvis at head strike) of the upper body may have occurred in test C4, and that may have also resulted from the pelvis getting trapped under the hood leading edge in C5. This discrepancy is believed to affect the T8 trajectories as well. The head resultant velocity at the time of head strike is slightly greater in test C4 than in test C5. This seems to be a result of the greater *x-z* plane rotation of the PMHS upper body seen in C4.

In the previous study, the Polar-II dummy was shown to generally replicate the PMHS kinematics in impacts with a small sedan by remaining within 10 % path length corridors (Kerrigan *et al.*, 2005). In the current study, however, the dummy's head, top of thorax and thorax CG trajectories stay within narrower corridors (k=5%). Conversely, a great discrepancy between pelvis trajectories in the PMHS tests provides for an average trajectory and corridor very different from the dummy response. While the dummy appears to more closely mimic the kinematics of PMHS C5, the dummy pelvis still appears to penetrate and deform the hood leading edge more than the PMHS. Much greater damage to the hood leading edge was seen in the dummy tests than in PMHS test C4. The greatest damage to the hood leading edge and upper grill of the SUV was seen in test C5, likely due, again, to a combination of the initial height of the pelvis CG and the mass of PMHS C5 (104 kg).

Although there is a difference in the peak head resultant velocity and the timing of the peak head resultant velocity between the PMHS tests and the Polar-II tests with the SUV, the velocities at head strike are similar (7.1-8.8 m/s for the PMHS and 8.1-8.3 m/s for the dummy). The difference in head resultant velocity at head strike between the PMHS and dummy in the sedan tests was partially attributed to the lack of active musculature in the PMHS neck (Kerrigan *et al.*, 2005). After examining the video images (Figure 5), it became apparent that the lack of muscle tension in the neck caused the head of the PMHS to be close to or even touching the left shoulder at 60 ms. However, in the dummy tests, the increased neck stiffness caused the head to rotate with the thorax earlier preventing the head from getting close to the left shoulder. Since the same effect was hypothesized to be a cause of head velocity differences in the PMHS tests, it is now believed that more sliding up the vehicle hood by the PMHS than the dummy is a more likely cause for head velocity discrepancies in the sedan tests.

The biggest difference between PMHS and Polar-II kinematics is that the dummy trajectories are shorter than the PMHS trajectories and thus the WAD to head strike is lower for the dummy. One explanation of this is that the dummy, in the striding mid-stance gait posture, was shorter than the PMHS in the pre-test orientation. A second explanation could be that in the absence of active musculature, the PMHS spine is permitted to stretch more than is possible in the dummy. This stretching could explain why PMHS trajectory lengths are greater than dummy trajectory lengths. However, without additional testing the relative contribution of this factor is unknown.

A third reason for this discrepancy could be that the pre-test position of the PMHS was slightly different than that of the Polar-II. Four goals were used to position the dummy and PMHS lower extremities in a mid-stance gait position before each test:

[1] both right and left thighs should be at the same angle with respect to the ground and no more than 85 degrees from horizontal,

[2] both feet should be on the ground with the back of the right heel and the front of the left shoe tip equidistant from the pedestrian sled center line (and the vehicle center line),

[3] with the right leg (struck side) back and left leg forward, and

[4] with both knees at 0 degrees flexion.

There were problems achieving this "goal" stance with both the dummy and the PMHS. In the dummy, limitations in hip joint range of motion restricted extension of the right (struck-side) hip. Once the hip had been maximally extended (~5 degrees with respect to the thorax), the left hip was flexed a similar magnitude. To achieve goal [2], it was then necessary to push the pelvis of the dummy back, creating an angle of the thorax with respect to the ground (Figure 4). Although this angle was not directly measured, photo graphic analysis suggests that the dummy spine could have been as much as 10-15 degrees from vertical.

Achieving the goal stance with the PMHS was more difficult than with the dummy. The PMHS hip and knee joints were much less stiff over their natural range of motion than that of the dummy's joints. This made it impossible to put the right hip into extension because the right thigh was drawn forward into a vertical position by gravity. Artificially supporting the knee joint could have solved this problem, but it would have resulted in stiffening the knee joint. It was determined that any artificial stiffeners may affect surrogate kinematics, and thus should not be used. Since the lack of joint

stiffness allowed for gravity to dominate the position, positioning goals [1] and [4] were impossible to achieve in both lower extremities. Positioning goal [2] was achieved by allowing the right knee to remain flexed and the left knee to stay at 0 degrees flexion. However, it was necessary to tape the right heel of the PMHS to the pedestrian sled to keep it flat against the simulated ground level (this tape was later pre-cut to permit easy tearing during the collision). The upper body's force held the left knee at 0 degrees flexion allowing for partial achievement of positioning goal [4]. Since the orientation of the lower extremities did not require any readjustment of the PMHS torso, the torso was always oriented vertically. Although differences exist in the initial position of both the dummy and PMHS, additional testing is necessary before concluding that differences in initial position cause differences in trajectory lengths.

Finally, surrogate kinematics were compared between the SUV and the sedan using previously published data (Kerrigan *et al.*, 2005). The first obvious conclusion is that pedestrian kinematics are highly sensitive to vehicle geometry. Secondly, it is clear that the dummy predicts a similar level of kinematic sensitivity to vehicle shape as the PMHS. The dummy and PMHS depict a larger difference in trajectory length when tested with an SUV as opposed to being tested with a small sedan (Figure 15). An explanation for this difference in trajectory length between the dummy and PMHS is related to how much the surrogate slides up the vehicle prior to head strike. In the previous study, the PMHS were shown to slide up the hood more than the dummy (Kerrigan *et al.*, 2005). There is no evidence for sliding in the SUV tests since for both the dummy and PMHS, the legs are still pinned under the bumper at the time of head strike, which restricts sliding. Thus, greater sliding by the PMHS in the sedan tests could cause the difference in time of head strike between the dummy and PMHS in the sedan tests (128-152 ms) that is absent in the SUV tests (96-100 ms).

It is interesting to note that the PMHS predicts a difference in head velocity at head strike between the SUV and the sedan, but the dummy predicts a smaller difference (Figure 15). One element of this difference is that the head velocity of the dummy is clearly decreasing at the time of head strike in the sedan tests, but the same is not true for PMHS in sedan tests. Lack of active neck musculature could also play a role in creating this difference but that does not explain why the difference between PMHS and dummy is greater in the sedan tests than in the SUV tests. This could be justified again by examining sliding at the pelvis-hood contact. Since there is a greater difference in sliding between the PMHS and the dummy in the sedan tests than in the SUV tests, this could cause a greater discrepancy in head velocity for the sedan tests than the SUV tests. More testing an analysis is required before a conclusion regarding the velocity discrepancies can be attained.

Finally, according to an epidemiology study, pedestrians struck by an SUV as compared to a passenger car are twice as likely to sustain brain injury (Ballesteros *et al.*, 2004), but the source of injury for pedestrians struck by an SUV is the hood whereas it is the windshield for passenger cars (Longhitano *et al.* 2005). Since both the dummy and PMHS predict that the head velocity at head strike for a sedan is greater than the head velocity at head strike for an SUV, greater stiffness of the hood and engine components below is likely the cause of increased potential for head injury. To show this, a comparison of head acceleration traces at head strike and HIC values should be made.

CONCLUSION

Although the kinematic biofidelity of the Polar-II dummy had already been evaluated in impacts with a small sedan, it was hypothesized that pedestrian kinematics were highly sensitive to vehicle geometry. Thus, to evaluate the kinematic biofidelity of the dummy in SUV impacts, full scale pedestrian impact experiments with PMHS and the Polar-II pedestrian dummy were performed using a mid-sized SUV. Overall, these experiments showed that pedestrian kinematic response is highly sensitive to vehicle front-end geometry.

Additionally the Polar-II dummy proved to have kinematic repeatability and to be generally biofidelic in that the trajectories of the head, T1, and T8 all fit within the path length corridors. Since the kinematic response of the Polar-II dummy was found to fit within wider corridors in the sedan tests, based solely on trajectory of the head, T1 and T8, it can be concluded that the Polar-II dummy exhibits higher kinematic biofidelity in impacts with an SUV than with a sedan. Pelvis trajectory in SUV impacts was determined to be highly sensitive to initial pelvis height. Similarity of head resultant velocities at impact between the PMHS and dummy suggest that the Polar-II can also accurately predict head resultant velocity at head strike for a PMHS. The head resultant velocity in

impacts with an SUV was shown to be somewhat lower than the colliding vehicle's velocity for tests at 40 km/h. Finally, head resultant velocities at the time of head strike were also shown to be lower in impacts with an SUV than in impacts with a small sedan.

REFERENCES

Akiyama A, Okamoto M, Rangarajan N. (2001) Development and application of the new pedestrian dummy. NHTSA, Paper 463, Proc. 17th Conference on the Enhanced Safety of Vehicles, Amsterdam, The Netherlands.

Akiyama A, Yoshida S, Matsuhashi T, Moss S, Salloum M, Ishikawa H, Konosu A. (1999a) Development of human-like pedestrian dummy. Paper 9934546, Japanese Society of Automotive Engineers, Chiyoda-Ku, Tokyo, Japan.

Akiyama A, Yoshida S, Matsuhashi T, Rangarajan N, Shams T, Ishikawa H, Konosu A. (1999b) Development of simulation model and pedestrian dummy. Paper 1999-01-0082, Society of Automotive Engineers, Warrendale, PA.

Artis M, Mcdonald J, White R, Huang TJ, Shams T, Rangarajan N, Akiyama A, Okamoto R, Yoshizawa R, Ishikawa H. (2000) Development of a new biofidelic leg for use with a pedestrian dummy. Proceedings of the 2000 International Conference on the Biomechanics of Impacts (IRCOBI), Montpellier, France.

Ballesteros M, Dischinger P, Langenberg P. (2004) Pedestrian injuries and vehicle type in Marlyland, 1995-1999. Accident Analysis and Prevention 36 (2004), pp. 73-81.

Bourret P, Farisse J, Seriat-Gautier B, Larousse R, Billault P, Ramet M, Cesari D, Cavallero C. (1979). Experimental study of injuries observed on pedestrians. Proceedings of the 1979 International Conference on the Biomechanics of Trauma (IRCOBI), Göteborg, Sweden, pp. 263-274.

Community Road Accident Database (CARE). EUROPA, European Commision, Transport. http://europa.eu.int/comm/transport/care/statistics/most_recent/detailed_breakdown/index_en.htm. 2002. (accessed 15 Apr 2004.)

Crandall J. (1994) The Preservation of Human Surrogates for Biomechanical Studies. PhD Dissertation, University of Virginia Department of Mechanical and Aerospace Engineering, Charlottesville, VA.

European Enhanced Vehicle-Safety Committee, "EEVC Working Group 17 Report—Improved Test Methods to Evaluate Pedestrian Protection Afforded by Passenger Cars," www.eevc.org, December 1998.

Heger A, Appel H. (1981). Reconstruction of pedestrian accidents with dummies and cadavers. NHTSA, Proc. 8th International Technical Conference on Experimental Safety Vehicles. pp. 836-841.

Huang TJ, McDonald J, Artis M, Rangarajan N, Shams T, White R, Beach D, Campbell R. Akiyama A, Yoshida S, Ishikawa H, Konosu A. (1999) Development of a biofidelic dummy for car-pedestrian accident studies. 1999 International Conference on the Biomechanics of Impacts (IRCOBI), Stiges, Spain.

Ishikawa H, Kajzer J, Schroeder G. (1993). Computer simulation of the impact response of the human body in car pedestrian crashes. Paper 933129, Proc. 37th Stapp Car Crash Conference, pp. 235-248.

ISO TC 22/SC 22/WG 22. Motorcycles—test and analysis procedures for research evaluation of rider crash protective devices fitted to motorcycles—Part 4: Variables to be measured, instrumentation, and measurement procedures. ISO/DIS 13232-4, August 31, 2004, Copyright ISO, Geneva, Switzerland, 2004.

ISO TC 22/SC 22/WG 22. Motorcycles—test and analysis procedures for research evaluation of rider crash protective devices fitted to motorcycles—Part 5: Injury indices and risk/benefit analysis. ISO/DIS 13232-4, September 7, 2004, Copyright ISO, Geneva, Switzerland, 2004.

Kallieris D, Schmidt G. (1988). New aspects of pedestrian protection loading and injury pattern in simulated pedestrian accidents. Paper SAE 881725. Proc. 32nd Stapp Car Crash Conference, pp. 185-196. Society of Automotive Engineers, Warrendale, PA.

Kam C, Kerrigan J, Meissner M, Drinkwater C, Murphy D, Bolton J, Arregui C, Kendall R, Ivarsson J, Crandall J, Deng B, Wang JT, Kerkeling C, Hahn W. (2005) Design of a full-scale impact system for analysis of vehicle pedestrian collisions. Paper 2005-01-1875, Society of Automotive Engineers, Warrendale, PA.

Kerrigan JK, Murphy DB, Drinkwater DC, Kam CY, Bose D, Crandall J. (2005) Kinematic corridors for PMHS tested in full-scale pedestrian impact tests. NHTSA, Paper 05-0394, Proc. 19th Conference on the Enhanced Safety of Vehicles (ESV), Washington DC, United States. Updated version of this manuscript available at www.centerforappliedbiomechanics.org/download/ESV_Update.pdf

Longhitano D, Henaray B, Bhalla K, Ivarsson J, Crandall J. (2005) Influence of vehicle body type on pedestrian injury distribution. Preliminary Paper number 05B-409, Society of Automotive Engineers, Warrendale, PA.

Lessley D, Crandall J, Shaw G, Kent R, Funk J. (2004) A normalization technique for developing corridors from individual subject responses. Paper 2004-01-0288, Society of Automotive Engineers, Warrendale, PA.

Okamoto Y, Akiyama A, Okamoto M, Kikuchi Y. (2001) A study of the upper leg component tests compared with pedestrian dummy tests. NHTSA, Paper 380, Proc. 17th Conference on the Enhanced Safety of Vehicles (ESV), Amsterdam, The Netherlands.

National Highway Traffic Safety Administration. (2003) Traffic Safety Facts 2003-Pedestrians, DOT HS 809 769, 2003.

National Police Agency (Japan). Traffic Accidents Situation 2003. Fatalities by Age Group and Road User Type. http://www.npa.go.jp/english/index.htm. 2003. (Accessed 12 Apr. 2004.)

Pritz H. (1978) Comparison of the dynamic responses of anthropomorphic test devices and human anatomic specimens in experimental pedestrian impacts. Paper 780894, Society of Automotive Engineers, Warrendale, PA.

Takahashi Y, Kikuchi Y, Okamoto M, Akiyama A, Ivarsson J, Bose D, Subit D, Shin J, Crandall J. (2005) Biofidelity evalutation for the knee and leg of the Polar pedestrian dummy. NHTSA, Paper number 05-0280, Proc. 19th Conference on the Enhanced Safety of Vehicles (ESV), Washington DC, United States.

World Bank (2001) Road Safety. http://www.worldbank.org/transport/roads/safety.htm (Accessed 12 Apr. 2004).